

Gradient surface porosity in titanium dental implants: relation between processing parameters and microstructure

M. G. KUTTY, S. BHADURI, S. B. BHADURI

School of Materials Science and Engineering, Clemson University, Clemson, South Carolina 29634, USA

E-mail: murali@clemson.edu

To be successful, an implant should be biocompatible, strong and contain surface pores to promote osseointegration. A one-step microwave sintering procedure of titanium powders was attempted in this work. The idea was to take advantage of the peculiar way microwave couple with metallic powders, i.e. generating heat in the interior of the sample and dissipating it away through the surface. This non-conventional heating of titanium powder produced a dense core with surface porosity. The dense core provides the strength while the surface pores promote bone growth. The experiments were carried out in a semi-industrial grade microwave cavity using a α -SiC susceptor. Power levels of 1–1.5 kW, and soaking periods of approximately 30 min were used. Microstructural characterization was carried out by a scanning electron microscope. The sintered titanium had gradient porosity on the surface with a thickness of about 100–200 μm depending on the microwave power. The pores were interconnected with size ranging from 30 to 100 μm . This kind of microstructure is favorable for cell growth. Tensile strength values as high as 400 MPa were obtained for these samples.

© 2004 Kluwer Academic Publishers

1. Introduction

Titanium and titanium-based alloys are widely used as materials for oral, maxillofacial, and orthopedic implants because of their advantageous mechanical properties and biocompatibility [1–5]. The ability of most bone tissues to intimately interact with the titanium surface is an important feature of the osseointegration phenomenon reported initially by Branemark and colleagues [1]. Lausmaa *et al.* [6] reported that the main reason for the biocompatible nature of the Ti surface and some of its alloys is the presence of TiO_2 on the surfaces. This so-called passive condition of titanium, when placed in a physiological environment allows for good corrosion resistance. Further, it was shown that the surface of titanium metal and its alloys become highly bioactive after being subjected to 5.0 M-NaOH treatment at 60 °C for 24 h and subsequent heat treatment at 600 °C for 1 h [7–9]. As a bioactive material, titanium and its alloys can bond chemically with bone, which accelerates the stabilization of implants and extends its lifetime before failure.

However, fixation of titanium implants is still a problem. Improper fixation impedes stress distribution at the implant bone interface, which can result in an interfacial failure and loosening of the implant with the possible consequence of fracture in the adjacent bone. It was found that rough titanium surfaces elicit a better local cellular response than smooth surfaces do [10, 11]. A macroporous titanium surface layer is often formed on

titanium and titanium alloy implants for morphological fixation of the implants to bone via bony in-growth into the porous structure. It has been shown that porous implants must have interconnected fenestrations to provide the space for vascular tissue required for continued mineralized bone growth [8]. The commonly accepted range of pore size is reported to be between 150 and 400 μm [12].

The initial technique used to form porous coating on the surface of the titanium was to sinter metal powder on the surface of dense solid. However, catastrophic changes such as microcracking and delamination were detected in the coatings due to the sintering process, resulting in a loss of strength [4, 13]. Another technique involved sintering titanium beads or fibers on the surface to create an interconnected network of pores. An electro-discharge compaction (EDC) fabrication technique was also used to produce commercially pure porous titanium dental implants [14–17]. In this technique, porous surface was produced by discharging a high voltage, high current density pulse of input energies through a column of loosely packed atomized titanium powders.

The most common technique to produce a porous surface is plasma spraying titanium powder on an implant to create macroporous titanium surface layer [18]. The plasma sprayed surfaces were reported to have advantageous morphological features that make it more suitable to successful clinical applications. However, this technique has several disadvantages. First, the geometry

of the interface between the porous coating and the substrate were found to cause stress concentrations that reduced the fatigue strength [19]. Second, high-temperature heat treatments often used to bond the porous coating and substrate, was attributed to changes in microstructure and eventual reduction in strength [20]. Lamellar structure, micropores, and microcracks have also been observed inside the plasma sprayed titanium coatings [21].

One of the major problems encountered in metallic implants, both coated and uncoated, is the stress shielding from residual bone which may result in detrimental restrictive bone remodeling so that long-term performance may be affected. Recently, work has been carried out to produce a functionally graded porous titanium coating that would be accompanied by a gradual change in the stiffness of the coating and allow for a better load transfer [18, 22]. The techniques mentioned in these references involve at least a two-step-processing route that increases the cost of the product. Other problems include contamination and the presence of impurity phases. This paper addresses these issues by utilizing a one-step microwave sintering process.

According to the common wisdom, metallic parts cannot be heated in a microwave. This is why sintering of metals in a microwave system is not so common. However, our preliminary experiments showed microwaves are coupled within the central portion of a metal powder compact and the heat generated is quickly dissipated away. This results in a gradient in temperature in a sample. This is how compacted metal powders and microwaves interact. So, microwave sintering of metal powders to full density is thought to be difficult task. While Roy *et al.* [23, 24] responded to this challenge very effectively we instead focused on utilizing the gradient in temperature generated during microwave exposure. Specifically, we took advantage of this temperature gradient in creating a graded porous structure [25].

Conventional sintering cannot produce the desired features for an implant, e.g. a dense core with surface pores. This present one-step processing of titanium produces the desired surface pore morphology for bone in-growth. The aim of this study is not only to create a graded structure, but also to establish the relationship between microwave parameters and the pore morphology.

2. Materials and methods

2.1. Sample preparation

Titanium powder used for this work was procured from Alfa Aesar (Wald Hill, MA) at a purity of 99.9% and particle size of -325 mesh. This mesh size was chosen since a finer powder would allow for better sintering under the fast sintering rates employed. The powder (about 7 g) was compacted at a pressure of 40 MPa and a hold time of 5 min into cylindrical disks of about 30 mm in diameter and 4 mm in thickness. The density values of these green compacts were determined by measuring the dimensions of the samples.

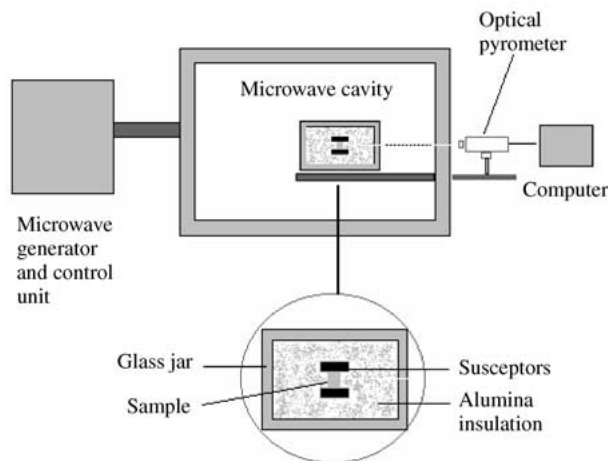


Figure 1 The set-up of the titanium sample and the SiC susceptor in the microwave.

2.2. Microwave processing

A semi-industrial microwave furnace (Microwave Materials Technology, MMT, Knoxville, TN) was used for densification. The system has a variable-power-output magnetron source capable of operating from 0 to 3 kW at 2.45 GHz. The experimental facility consisted of a microwave generator coupled to a cavity where samples were placed. The microwave cavity had a dimension 10 times the wavelength of electromagnetic radiation, which had a wavelength of about 12.5 cm. Hence this cavity was “overmoded.” The large sized cavity enhanced the mixing of the incoming microwave pattern with the reflected pattern.

The samples were placed in a flask made out of pyrex glass. The set-up is shown in Fig. 1. The flask also contained dense α -SiC that was used as a susceptor. Many materials do not couple well with microwave radiation at low temperatures. For effective microwave sintering they need to be preheated by conduction, convection or radiation from another source such as a flame, a heating element, or a microwave susceptor that couples with the microwave radiation. This is done until a high enough temperature is reached, after which the materials couple with the microwave radiation effectively. α -SiC, a microwave absorbing material, was used in this experiment to thermally heat the poorly absorbing titanium. Al_2O_3 insulator and fiberboard was used as insulation to prevent major heat loss. The flask was first evacuated and backfilled with Argon at atmospheric pressure. The titanium disks were sintered at 1.0, 1.25 and 1.5 kW for duration of 30 min. These settings were chosen based on earlier results reported elsewhere [25].

2.3. Temperature profile measurement

Temperature profile during sintering was obtained with a two-color pyrometer (Mikron L77, Mikron Inc. Oakland, NJ) with a temperature range of 900–3000 °C. Temperature data points were obtained with a data acquisition system. The pyrometer was focused on the sample surface in-between the susceptors through a hole created along the insulation material (Fig. 1).

2.4. Microstructure analysis

Fracture surfaces of the green compacts were observed under the Scanning Electron Microscope (Leo 1430) operating at 20 kV. Fracture surfaces were chosen since cutting the green body will alter the morphology of the green body. The sintered titanium disks were cut and mounted with the cut surface on the top to evaluate the morphology. This surface was first ground with coarse SiC paper and polished to 1 μm and observed under a scanning electron microscope (SEM) and an optical microscope (Leco, Olympus PMG3, St. Joseph, MI) to evaluate the extent of porosity and the microstructure.

2.5. Evaluation of content of pores

The porous surface on the titanium was analyzed via a digital imaging technique. SEM images were taken of the porous layer, each covering a depth of approximately 50 μm . A sequence of images from the surface through the interior was taken to provide the full depth profile. A commercial software (Adobe PhotoShop 6.0, Adobe Systems Inc.) was subsequently used to create a high contrast image with the pores designated as black regions and the dense as white. The contrast threshold was set such that the edges of the pores became regions of pure black, while the dense material remained white. The software was employed to generate a histogram of the percentage of black to white across each pixel line of the image. This was used to determine the percentage of pore space through the sample. For each sample, data were generated from six separate images to obtain an average value.

2.6. Tensile strength measurement

The tensile testing was conducted using a SATEC Model T 5000 Materials Testing Machine with a 5000 lb load cell. The software used to collect the data was a model 2000 A/D converter Digital Strain Indicator. A cross-head speed of 0.1 mm/s was used.

3. Results and discussion

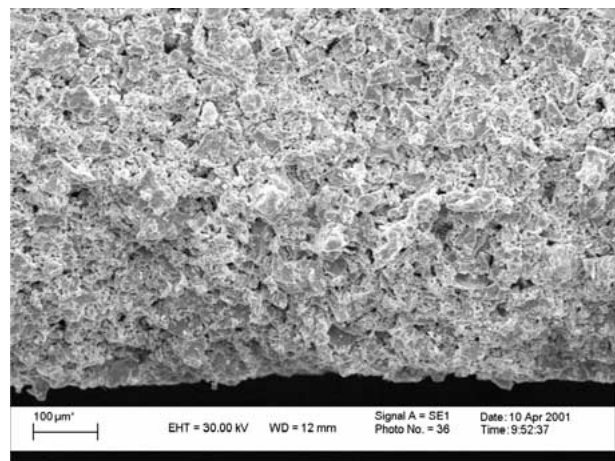
3.1. Green compact

The relative density of the green titanium compacts was 54.2%. This relative value was calculated by taking the theoretical value to be 4.5 g/cm³. The cross section of a green compact was observed under scanning electron microscope to determine if the gradient pores were due to the compaction of the powder that is achieved via uniaxial press. Fig. 2 shows a schematic of the examined region.

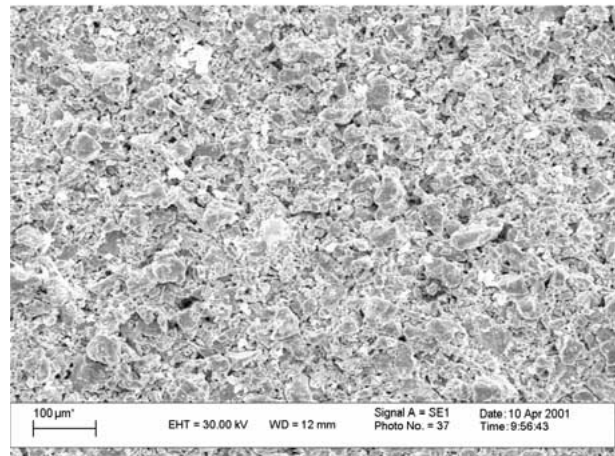
Fig. 3(a)–(c) show the morphology of the compact at the bottom, middle and the top of the sample. These clearly indicated the presence of a uniform porous



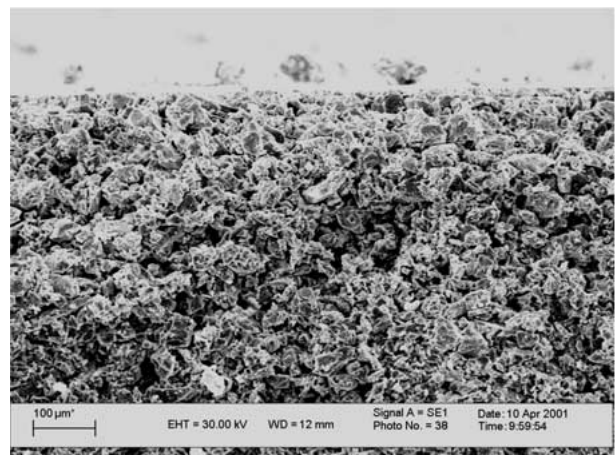
Figure 2 Schematic of the cut Ti sample and the position of the surface observed via SEM.



(a)



(b)



(c)

Figure 3 (a) Bottom region of green Ti compact; (b) Middle region of green Ti compact; (c) Top region of green Ti compact.

distribution. No signs of gradient porosity were observed near the surface of the sample.

3.2. Temperature measurement

The thermal history of the various runs are shown in Fig. 4 and Table I, respectively. The profile for run A (1.00 kW) showed the temperature of the sample increase in a linear manner until 1100 °C. After this point it gradually reached a plateau with a maximum temperature of 1220 °C in 22 min. This temperature remained constant until the microwave was switched off after 30 min. The sudden drop in temperature of the titanium

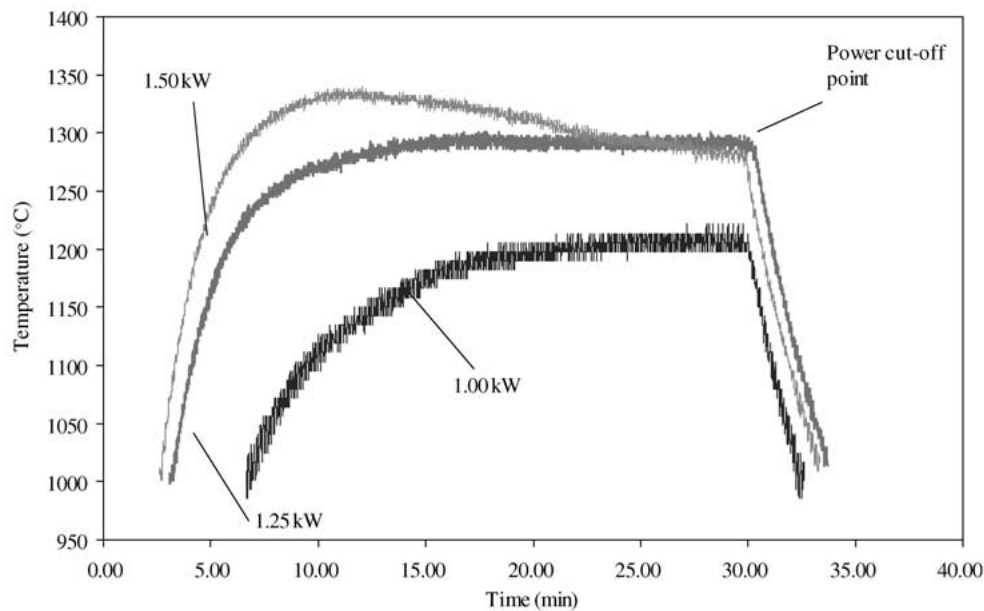


Figure 4 Temperature profile of sample sintered at 1.00, 1.25 and 1.50 kW for 30 min.

TABLE I Summary of thermal histories of sintering runs

Run no.	Microwave power (kW)	Maximum temperature/time taken ($^{\circ}\text{C}/\text{min}$)	Temperature after 10 min ($^{\circ}\text{C}$)	Temperature after 20 min ($^{\circ}\text{C}$)	Temperature after 30 min ($^{\circ}\text{C}$)
A	1.00	1220/21	1100	1200	1220
B	1.25	1300/17	1270	1300	1300
C	1.50	1340/11	1335	1320	1280

sample marked this point. The cooling was observed to occur rapidly and depended considerably on the amount of insulation surrounding the sample and susceptors.

The temperature profile of the samples sintered run B (1.25 kW) showed a similar trend as in run A. However, it reached a maximum temperature of 1300°C after just 17 min held for the remainder of the experiment. However, the sample sintered in run C (1.5 kW) had a rather different temperature profile as compared to the previous two profiles. The sample reached a maximum temperature of 1340°C within 10 min. This temperature started to drop gradually with time and reaches 1280°C after 30 min when the system was switched off. This observation is believed to be due to the radiation of heat from the sample and susceptors.

Compared with the melting point of pure titanium (1943°C), the temperatures obtained in the microwave experiments are lower. However, the temperatures measured were on the surface of the sample where heat loss is greater as compared to the center of the sample. It is possible that there is an increase of temperature from the surface to the center. This is a common observation in samples sintered in the microwave unit due to the nature of the heating, as alluded to before.

3.3. Microstructure observation of sintered sample

Fig. 5(a) shows the gradient porosity that was found in the sintered samples. This SEM micrograph shows the

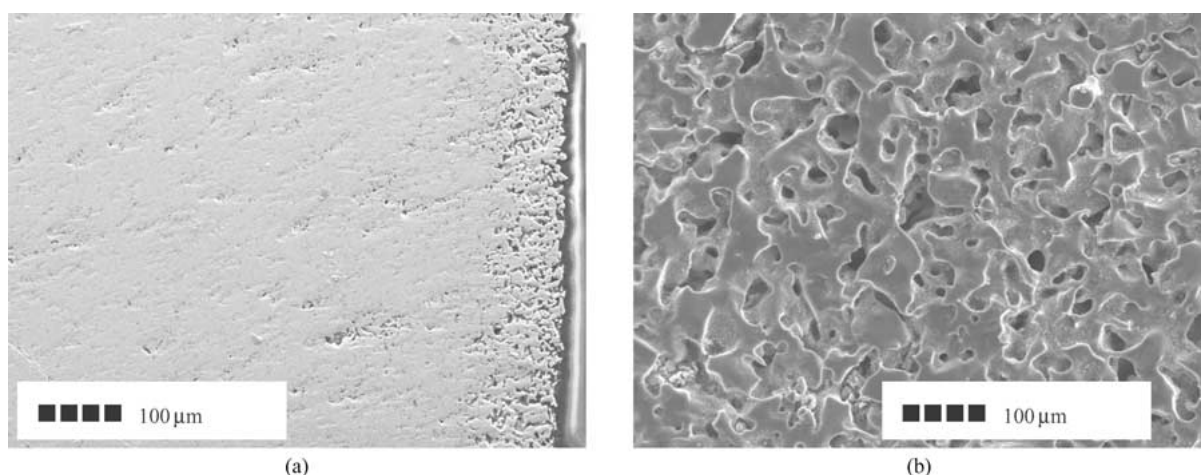


Figure 5 (a) shows the gradient porosity at the surface of the Ti sample and (b) is the interconnected pores as seen from a planner view.

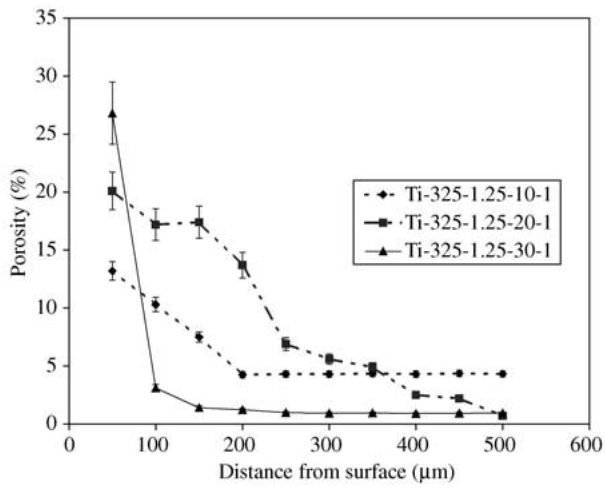


Figure 6 The change in porosity of the - 325 mesh sample with distance from surface.

change in both distribution of pores and the change in size of pores. The border between the porous region and the dense region is evident. Both temperature and duration of sintering run control the thickness of this layer.

Fig. 5(b) shows the surface feature of the sintered sample. It is clear from this picture that the pores are interconnected since it was possible to see through a considerable depth of the sample. The pore size is controlled mainly by the size of the powders used. The general pore size is from 30 to 100 μm.

3.4. Evaluation of content of pores

The graph (Fig. 6) shows the change in porosity percentage with distance from surface. The highest porosity near the surface is observed in the sample with sintering time of 30 min with a value of 27%. However

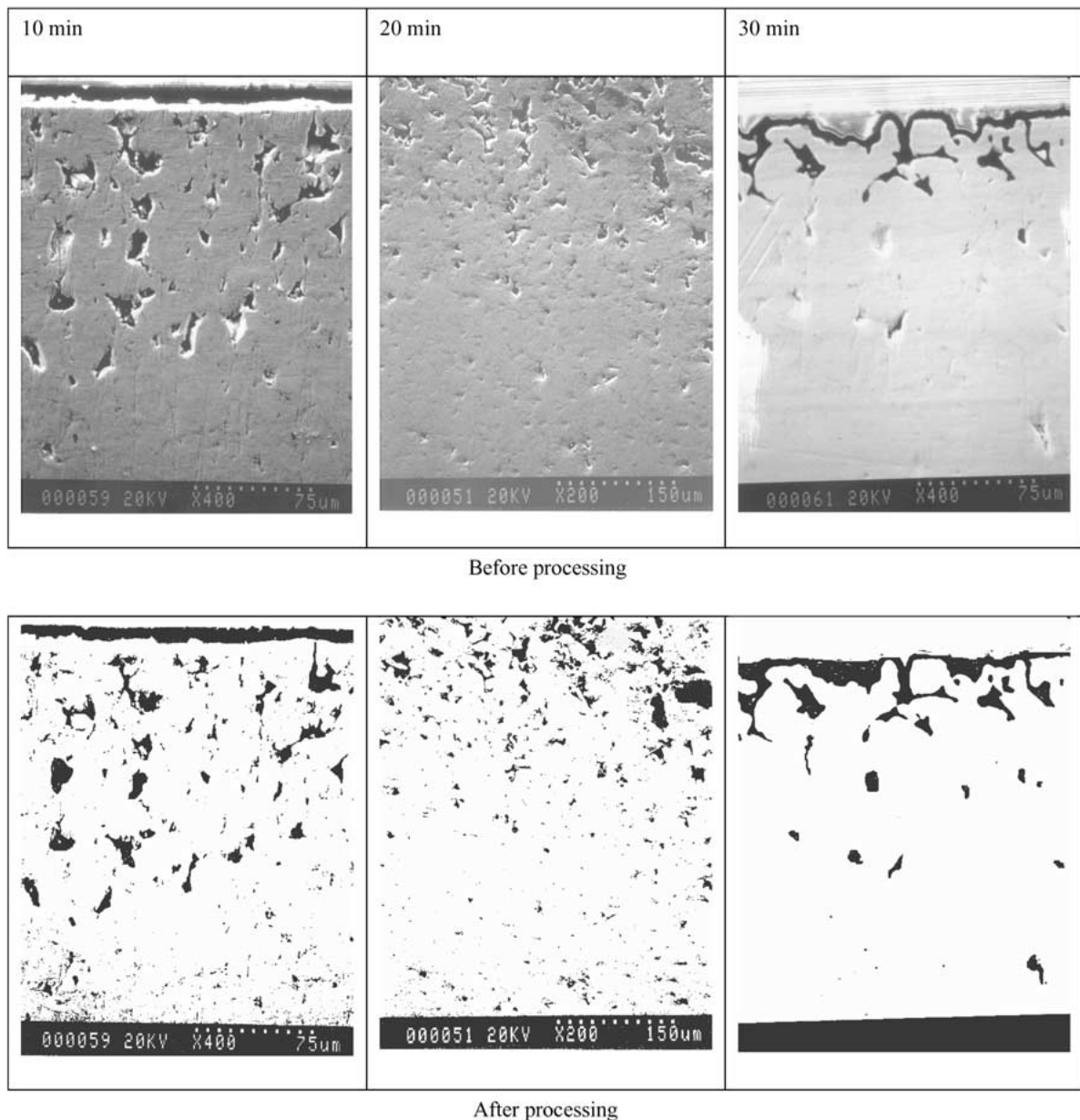


Figure 7 Indication the change in porosity with depth for - 325 mesh sample sintered at 1.25 kW and various duration.

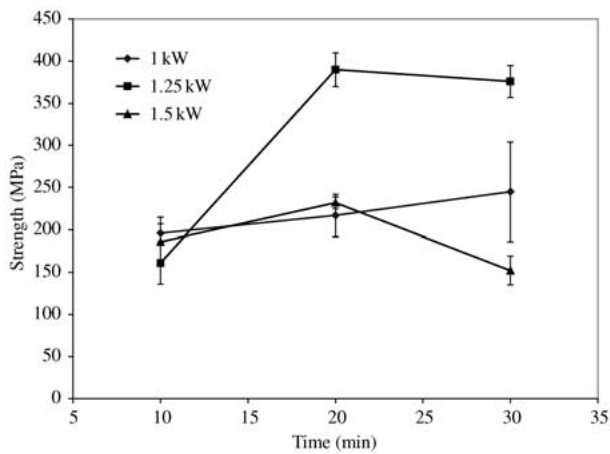


Figure 8 Change of tensile strength with sintering time for the titanium samples sintered at different microwave power.

this drops significantly to 3% at 100 μm and reaches a plateau at 1 μm . The sample sintered at 10 min shows a similar trend, dropping from 13 to 4 μm . However the sample sintered at 20 min shows a gradual change in porosity from the surface, with a value of 20 μm , to 0.7 μm at 500 μm from the surface.

The general trend shown by the Ti sample sintered for 10 and 30 min is similar. The sudden drop in porosity or increase in density after a certain depth is due to the heat lost near the surface via radiation. The sintering time plays an important role in determining the depth of the porous region and the final density achieved by the bulk material. The temperatures measured at the surface indicate that density above 90% of theoretical is easily attainable by this process (Fig. 7).

3.5. Tensile testing

The tensile testing conducted shows that the samples sintered at 1.25 kW for 20 min have the highest strength with values exceeding 400 MPa (Fig. 8). This value is within the reported values for bulk CP titanium with values ranging from 345 to 550 MPa. The strength increases dramatically when sintering time is increased from 10 to 20 min but shows a slight drop when it is further increased to 30 min. This is believed to be due to the surface damage observed in the latter sample. Cracks were present at the interface of the porous region and the dense region in these samples.

4. Conclusions

The results indicate that it is possible to obtain a graded porosity on the surface while maintaining a dense core in a titanium sample via a one-step microwave-processing route. The thickness of the porous region is 100–200 μm and the pore size is approximately 30–100 μm . This makes it an ideal surface for osteoblast cell growth. Furthermore, the gradient porosity and the graded nature

of the change from dense material to porous surface should provide with a better stress transfer than a coated surface. This was achieved without sacrificing the strength. The potential of this, one-step processing technique to produce various implants, other than dental is also unlimited.

Acknowledgment

This work is supported by NSF-DMII-0085100.

References

1. P. I. BRANEMARK, R. ADELL, T. ALBREKTSSON, U. LEKHOLM and S. LUNDQUIST, *Biomaterials* **4** (1983) 25.
2. J. C. KELLER, C. M. STANFORD, J. P. WIGHTMAN, R. A. DRAUGHN and R. ZAHARIAS, *J. Biomed. Mater. Res.* **28** (1994) 939.
3. J. E. DAVIES, B. LOWENBERG and A. SHIGA, *ibid.* **24** (1990) 1289.
4. K. ASAOKA and N. KUWAYAMA, *ibid.* **19** (1985) 699.
5. T. KURACHI, H. NAGAO, H. NAGURA and S. ENOMOTO, *Arch. Oral Biol.* **42** (1997) 465.
6. T. NOMURA, S. SHINGAKI and T. NAKAJIMA, *J. Long-term Effects Med. Implants* **8** (1998) 175.
7. T. KOKUBO, *Acta Mater.* **46** (1998) 2519.
8. H. KIM, T. KOKUBO, S. FUJIBAYASHI, S. NISHIGUCHI and T. NAKAMURA, *J. Biomed. Mater. Res. (USA)* **52** (2000) 553.
9. YOSHIKI OSHIDA, U.S. Patent No. 6183255, "Titanium Material for Implants" (2001).
10. H. ZREIQAT and C. R. HOWLETT, *J. Biomed. Mater. Res.* **47** (1999) 360.
11. J. LAUSMAA, M. ASK, U. ROLANDER and B. KASEMO, *Mater. Res. Soc. Symp. Proc.* **110** (1989) 647.
12. R. A. AYERS, S. J. SIMSKE, T. A. BATEMAN, A. PETKUS, R. L. C. SACHDEVA and V. E. GYUNTER, *J. Biomed. Mater. Res.* **45** (1999) 42.
13. D. WOLFARTH and P. DUCHEYNE, *ibid.* **28** (1994) 417.
14. M. I. LIFLAND, D. K. KIM and K. OKAZAKI, *Clin. Mater.* **14** (1993) 13.
15. J. QUI, J. T. DOMINICI, M. I. LIFLAND and K. OKAZAKI, *Biomaterials (UK)*, **18** (1997) 153.
16. M. I. LIFLAND and K. OKAZAKI, *Clin. Mater.* **17** (1994) 203.
17. K. OKAZAKI, D. K. KIM and R. A. KOPCZYK, Conference Science and Engineering of Light Metals. RASELM '91 (Tokyo, Japan, 1991) 103.
18. Y. Z. YANG, J. M. TIAN, J. T. TIAN, Z. Q. CHEN, X. J. DENG and D. H. ZHANG, *J. Biomed. Mater. Res.* **52** (2000) 333–337.
19. D. DE SANTIS, C. GUERRIERO, P. F. NOCINI, A. UNGERSBOCK, G. RICHARDS, P. GOTTE and U. ARMATO, *J. Mater. Sci. Mater. Med.* **7** (1996) 21.
20. D. H. KOHN and P. DUCHEYNE, *J. Biomed. Mater. Res.* **24** (1990) 1483.
21. C. K. CHANG, J. S. WU, D. L. MAO and C. X. DING, *ibid.* **56** (2001) 17.
22. M. THIEME, K. P. WIETERS, F. BERGNER SCHARNWEBER, H. WORCH, J. NDOP, T. J. KIM and W. GRILL, *J. Mater. Sci. Mater. Med.* **12** (2001) 225.
23. R. ROY, D. AGRAWAL, J. CHENG and S. GEDEVANISHVILI, *Nature* **399** (1999) 668.
24. R. ROY, D. K. AGRAWAL, K. DINESH and J. CHENG, U.S. Patent No. 6,183,689 (2001).
25. M. G. KUTTY, S. BHADURI, J. R. JOKISAARI and S. B. BHADURI, *Ceram. Eng. Sci. Proc.* **22** (2000) 587.

Received 7 April 2002

and accepted 5 August 2003